NACA TN 4252 10593

TECH LIBRARY KAFB, NM
0066791

NATIONAL ADVISORY COMMITTEE FOR AERONAUTICS

TECHNICAL NOTE 4252

EXPERIMENTAL INVESTIGATION OF AN IMPULSE-TYPE SUPERSONIC COMPRESSOR ROTOR HAVING A TURNING OF 73° AT THE MEAN RADIUS

By James R. Sterrett

Langley Aeronautical Laboratory
Langley Field, Va.

Washington
June 1958

AFMDC
TECH LIBRARY
AFL 2811

TECH LIBRARY KAFB, NM
0066791

B

NATIONAL ADVISORY COMMITTEE FOR AERONAUTIC

TECHNICAL NOTE 4252

EXPERIMENTAL INVESTIGATION OF AN IMPULSE-TYPE SUPERSONIC COMPRESSOR ROTOR HAVING A TURNING OF 73° AT THE MEAN RADIUS

By James R. Sterrett

SUMMARY

A 16-inch-diameter supersonic impulse rotor with guide vanes was designed and tested in Freon-12. The rotor had inlet and exit hub-tip radius ratios of 0.575 and 0.75, respectively. The blade-passage design was based on the two-dimensional vortex-flow theory modified to account partially for the three-dimensional compressions.

Near the design tip speed of 662 ft/sec in Freon-12 (equivalent air value of 1,450 ft/sec) and open throttle conditions, the rotor produced a stagnation-pressure ratio of 7.2 and an efficiency of 90 percent with an equivalent weight flow of 28.6 lb/sec of air per square foot of frontal area. The efficiency at minimum back pressure was approximately constant at 90 percent for all speeds. The stagnation-pressure ratio decreased with increasing back pressure. The maximum-back-pressure condition at design speed resulted in a pressure ratio of 5.4 and an efficiency of 77.5 percent. For high efficiency, a stator must therefore operate without imposing a high back pressure on the rotor. The average exit Mach number at design speed and minimum back pressure was approximately 2.4 at an average discharge angle of 45°. The operating conditions were not accurately predicted by the design method, but the resulting rotor imparts a large work output to the fluid in the form of kinetic energy. The exit conditions for this rotor appear to be sufficiently uniform in flow angle, Mach number, and total pressure to allow possible efficient recovery in the stators.

INTRODUCTION

The potentiality of the impulse supersonic compressor to produce very high pressure ratio per stage has created considerable interest in its use for turbojet engines. In this type of compressor, the flow is

turned through a very large angle with little or no pressure rise. The flow leaving the rotor is supersonic and must be diffused in the stator where the kinetic energy imparted by the rotor is converted to static pressure. The demand for high-performance compressors in aircraft propulsion has initiated several theoretical and experimental studies of the supersonic impulse rotor. (For example, see refs. 1 to 9.) None of the existing methods of design has resulted in an accurate prediction of the operation of a supersonic impulse rotor.

The performance values of the impulse rotors alone given in references 8 and 9 were good; however, attempts to recover the kinetic energy by placing stators behind the rotor have generally resulted in poor stage performance. Even though the successful design of stators seems to be the major problem in supersonic impulse compressors, the design of efficient rotor sections remains important since poor flow conditions leaving a rotor would increase the difficulty of obtaining good pressure recoveries in the stator.

The present paper is part of an investigation performed at the Langley Laboratory of the NACA in an effort to develop a supersonic impulse rotor with uniform exit flow and a design method which accurately predicts the operation of a supersonic impulse rotor. In the present study, an impulse rotor was designed by using a simplified quasi-three-dimensional design. The method used was to design sections which were effectively based on the two-dimensional vortex-flow theory (ref. 5) but modified to account partially for the compressions due to the three-dimensional flow. It was also desirable to develop a high-pressure-ratio impulse rotor which could be used to test stators for diffusing high Mach number flow.

The rotor-design method and the performance of the rotor alone are given in this report. The rotor was tested in Freon-12 gas over a speed range of 62 percent to 101 percent of design speed.

SYMBOLS

A	area, sq ft
C_p	specific heat at constant pressure, ft-lb/slug $^{\circ}F$
g	acceleration due to gravity (32.2 ft/sec^2)
M	Mach number

n	rotational speed of rotor, rps
P	stagnation pressure, lb/ft^2
p	static pressure, lb/ft^2
Q	torque, ft-lb
r	radial position measured from axis of rotation, ft
T	stagnation temperature, $^{\circ}R$
t	static temperature, $^{\circ}R$
ΔT	measured stagnation-temperature rise, $^{\circ}R$
$\Delta T'$	isentropic stagnation-temperature rise, $^{\circ}R$
U	rotational velocity of blade element, $2\pi rn$, ft/sec
V	velocity of fluid, ft/sec
W	weight flow, lb/sec
β	angle between axial direction and flow direction, deg
γ	ratio of specific heats
δ	ratio of inlet total pressure to standard sea-level pressure, $P_i/2,116$
η_m	momentum efficiency, $\dfrac{C_p \Delta T'}{U_2 V_{2,\theta} - U_1 V_{1,\theta}}$
η_Q	torque efficiency, $\dfrac{C_p \Delta T' W}{2\pi n Q g}$
η_t	temperature (adiabatic) efficiency, $\dfrac{\Delta T'}{\Delta T}$
θ	ratio of inlet stagnation temperature to standard sea-level temperature, $\dfrac{T_i}{518.6}$
ν	supersonic expansion angle, angle through which flow must expand from $M = 1.0$ to given Mach number, deg

ν' change in the supersonic expansion angle due to three-dimensional compressions, deg

ρ density, slugs/cu ft

σ solidity, Chord/Blade spacing

ϕ turning angle, deg

Subscripts:

e entrance condition

h hub

i settling chamber

t tip

z axial component

θ tangential component

1 rotor entrance

2 rotor exit

R indicates rotor coordinates

COMPRESSOR AERODYNAMIC DESIGN

Rotor Design

The rotor was designed for operation in Freon-12 gas. In the design of the 16-inch-diameter supersonic rotor, the following conditions were prescribed:

1. An impulse-type design (no static-pressure rise near the mean radial station)

2. A radially constant work input with an assumed efficiency of 90 percent

3. A rotational speed of 663 ft/sec in Freon at the tip radius, or an equivalent air tip speed of 1,450 ft/sec

4. An inlet hub-tip radius ratio of 0.575

5. An inlet absolute Mach number of 0.80 at the mean radius

6. Inlet guide vanes with a prescribed turning of 12° at the mean radius and radial free-vortex distribution of tangential velocity

7. A turning angle of approximately 73° at the mean radius

With these prescribed conditions, exit conditions were calculated by an iteration process to satisfy continuity. The resulting exit hub-tip radius ratio was 0.75. The velocity diagram is given in figure 1 for the tip, pitch, and root. The rotor has a design pressure ratio of 6.5 with a weight flow of 58.0 pounds of Freon-12 per second per square foot of frontal area, which is equivalent to 31.1 pounds of air.

Blade-Section Design

At the time this compressor was designed, no completely satisfactory method had been given in the literature for computing compressor blade sections taking into account the three-dimensional flow effects. The blade sections for this rotor were therefore designed using essentially a two-dimensional characteristic solution which had been modified partially to account for the three-dimensional effects. In the following discussion, it is often convenient to discuss the Mach number in terms of the supersonic expansion angle ν.

Small-angle wedges were used on the leading edge to create thicker leading edges. Since the upstream axial component of $M_{1,R}$ is subsonic, expansion and compression waves from the blades propagate upstream and the entrance Mach number and the flow direction within the blade are not the same as the undisturbed inlet condition. The undisturbed inlet conditions are given by the velocity diagrams, and the entrance Mach number and direction within the blade were calculated by the analytic method given in reference 5.

The blade sections were designed for the three radial stations (root, pitch, and tip sections). If the design entrance inlet-flow angle and the turning angle of the blades are known, the exit area normal to the flow for a sharp trailing edge can be obtained from the following equation:

$$\frac{A_1}{A_2} = \frac{\cos \beta_e}{\cos(\beta_e - \phi)}$$

The exit Mach number that would result from this two-dimensional-area change was determined assuming isentropic flow. Assuming these entering and exit conditions, two-dimensional preliminary blade sections were designed using the vortex-flow method given in reference 5. Blade passages designed by use of this method are bounded by two concentric arcs and the entering and exit transition sections. The Mach number is constant along any particular concentric arc. The Mach numbers chosen for the concentric arcs for these blades were determined by trial and error such that the sections had a solidity distribution which would yield a nearly constant chord length. Although the Mach numbers along the concentric arcs were, therefore, chosen rather arbitrarily, cascade tests have indicated that the pressure recovery for a vortex-flow type of blade is generally satisfactory and independent of surface Mach number if the section is capable of supersonic starting.

The final blade sections were obtained by redrawing the preliminary two-dimensional blade sections using quasi-three-dimensional characteristics. In order to accomplish this, the blade was first divided into equal axial-blade distances. Whenever a characteristics line crosses one of these axial segment lines, the flow direction remains the same as for the two-dimensional case, but the Mach number is changed by the amount of the three-dimensional supersonic-expansion-angle change ($\Delta\nu'$) calculated for that position. In the calculation of the value of $\Delta\nu'$, the following conditions were prescribed. The difference between the two-dimensional expansion-angle change calculated from the area change across the rotor and the desired velocity-diagram expansion-angle change across the rotor was assumed to result from three-dimensional effects and can be written as

$$\sum \Delta\nu' = \left(\nu_{2,R} - \nu_{1,R}\right)_{\text{two dimensional}} - \left(\nu_{2,R} - \nu_{1,R}\right)_{\text{velocity diagram}}$$

Since the hub is nearly a concave surface, the compression waves originating from the hub are assumed to accumulate at the rear of the blade passage and thus result in a parabolic distribution where

$$\nu' \propto Z^2$$

By the use of these two equations, $\Delta\nu'$ can be calculated at any axial segment line.

An illustrative example showing the corrected pitch section is shown in figure 2. In each bounded region of flow for this figure, two flow conditions are known; one is the flow direction β and the other is the supersonic expansion angle ν. The surface sections AB and CD, figure 2, are identical to those of the two-dimensional solution. Downstream of points B and D the surface is distorted compared to the

two-dimensional solution because of the arbitrary compressions assumed which increase the inclination of the Mach wave with respect to the flow direction to any given point; thereby, the location of the point on the surface at which such waves are reflected or canceled is changed. As a result of the distortion, the trailing edges of the sections are not sharp but terminate with a finite thickness. For the hub and mean sections, this thickness was small and desirable for fabrication. However, for the tip section, it was necessary to fair the rear portion of the surfaces in order to terminate the profile with a reasonable thickness.

From these sectional layouts, the three-dimensional cross-sectional flow area through the rotor blade was calculated. The hub contour was then faired in between entering and exit positions to insure that the three-dimensional flow area was always at least 90 percent of the entrance area. This was a sufficient area ratio for the starting criterion when an average entering Mach number of 1.48 was assumed.

After the rotor had been designed, a method for designing compressor blades using a three-dimensional characteristics system along a stream filament was obtained and is given in reference 10. The method of reference 10 was used to find the Mach numbers that would result along the tip section of the present rotor. The Mach numbers near the rear of the blade could not be found as the concave-surface Mach number became less than 1. When applying the calculation given in reference 10 to the present rotor, the streamline filament thickness was assumed to vary linearly through the rotor. Figure 3 shows a comparison of the Mach number distribution as calculated by the method of reference 10 and as determined by the quasi-three-dimensional process of this report. An examination of the figure reveals that while the two design methods do not give the same Mach number distribution, the two design methods produce distributions which show similar trends.

APPARATUS AND METHODS

Test Facility

A schematic diagram of the compressor stand is given in figure 4. This test stand is described in detail in reference 11. Freon-12 was used as the working fluid for these tests. The rotor is driven by a 3,000-horsepower induction motor through a 2:1 gear-ratio speed increaser. The motor drive shaft was adapted for a wire strain-gage type of torquemeter.

Test Compressor

The rotor was designed to have 35 blades. A schematic sketch of the blade and the hub contour is shown in figure 5. The coordinates of the compressor blades at the three design stations and the coordinates of the hub contour are given in table I and table II, respectively. A photograph of the rotor is presented in figure 6.

The rotor blades and the hub "buildup" were formed of fiber glass and polyester resin. The blades and hub buildup were pin fastened to a metal hub as shown schematically in figure 5. When the rotor was originally built, a piece of steel was inserted into the polyester resin to form the leading edge. This rotor failed structurally along the leading edge and was rebuilt without the steel insert.

The guide vanes were essentially circular arcs which were formed by shaping sheet steel. The annulus area of the guide vanes was larger than the rotor entrance area; thus, the possibility of choking the flow was reduced. There were 19 guide vanes, and their location, turning angles, and details are presented in figures 4, 1, and 7, respectively.

Instrumentation and Data Reduction

The instrumentation described in reference 11 was used to obtain the Freon-12 purity, the inlet flow conditions, the weight flow, and the static pressures on the inner and outer casings. A cylindrical-type probe was used to obtain the flow angle, total pressure, and static pressure at 10 radial positions behind the rotor. A calibrated chromel-alumel thermocouple rake was used to measure the total-temperature rise across the rotor. A photograph of these instruments is shown in figure 8. The survey stations, as shown in figure 4, are about $1\frac{3}{4}$ inches behind the rotor.

All pressures were measured by a multiple-tube mercury manometer board and were recorded simultaneously by photographing the manometer board. Commercial-type self-balancing potentiometers recorded the temperatures and the work input to the rotor as measured by a wire strain-gage type torquemeter.

The method of determining the performance of the compressor rotor and blade elements is given in reference 11. Some of the important factors that are useful in the understanding of this report are repeated herein for clarity.

The weight flow was obtained from a calibrated venturi and by an integration of the elemental weight flow at each radial station at the entrance and exit stations. In general, the values of the inlet weight flow were within 2 percent of that obtained by the venturi. The values of the exit weight flow were generally within 5 percent of that obtained by the venturi; however, the exit weight flow was sometimes 10 percent higher than that measured by the venturi. Only the weight flows obtained from the venturi are presented in this paper.

Considerable difficulty was encountered in obtaining the correct static pressure leaving the rotor, as indicated by the scatter in the measured values. From past experience, this has been encountered whenever the exit Mach number is highly supersonic. The static-pressure distributions used for all data presented in this paper were obtained by fairing the measured data obtained from the probe and the average of the readings of the wall static taps which showed the smallest variation of pressure with survey-probe position. The data for all tests at open throttle were faired to obtain a family of curves; similarly, all tests for closed throttle were faired as a family.

The values of C_p and γ that were used in the calculations were obtained for the measured Freon purity and the average temperature.

The efficiency was computed by two methods; one, η_Q, was based upon measured torque, and the other, η_m, was based upon the momentum change across the rotor. For the blade-element-efficiency calculations, the streamlines were assumed to exist between centers of equal-percentage annular area at the exit and entrance stations. The efficiency η_t, based on the total temperature, was not used because near the end of the test it was determined that the temperature rake was misalined and the rotor was damaged before the reruns could be completed.

The overall total-pressure ratios were computed from the inlet stagnation pressure which was measured in the settling chamber and a mass-weight average of the downstream total pressures which was corrected for normal shock-probe losses.

RESULTS AND DISCUSSION

Overall Performance

The total-pressure ratio across the rotor obtained at various speeds in Freon-12 is presented in figure 9(a). At 101 percent of design speed and minimum back pressure, a maximum-stagnation-pressure ratio of 7.2 was

obtained. The equivalent weight flow at this operating condition was approximately 73.0 lb/sec of Freon-12 or an equivalent air value of approximately 39.8 lb/sec. This corresponds to an approximate equivalent weight flow of 28.6 lb/sec of air per square foot of frontal area. At this rotational speed, the pressure ratio could be decreased somewhat by applying back pressure without a change in the weight flow; however, as the back pressure was further increased by closing the throttle valve, the weight flow decreased to 72.0 lb/sec of Freon-12.

A similar type of characteristic curve is obtained at the 91 percent design speeds. The vertical portion of the curve for the lower three speeds is very short if it exists at all. A decrease in the pressure ratio with increased back pressure is a characteristic of rotors which turns the flow past axial. The reason for this reduction can readily be seen from a typical velocity diagram (for example, fig. 1). As the back pressure is increased, there is a reduction in $M_{2,R}$, which (assuming $\beta_{2,R}$ remains constant) would result in a decreased tangential component of the absolute exit Mach number $(M_{2,\theta})$ and thus a decrease in the work input or available total-pressure ratio.

The torque efficiencies of the rotor obtained at various speeds are given in figure 9(b). The measured efficiency for the peak total-pressure ratio of 7.2 at 101 percent of design speed is approximately 90 percent. At the design speed, the efficiency decreased with increasing back pressure until at the stall point the efficiency had been reduced to 77.5 percent. At open throttle, the efficiency remains approximately constant at all speeds. At maximum-back-pressure condition, the efficiency dropped slightly with increasing speed; for example, the efficiency was 82.5 percent at 62 percent and 77.5 percent at 101 percent of design speed. For the three lowest speeds, the efficiency decreased with increasing back pressure and then increased with a further increase in back pressure. The cause of this variation of efficiency with back pressure will be discussed later.

The effect of back pressure on the static-pressure measurements along the rotor outer casing at 81 percent and 101 percent of the design speed is shown in figure 10. These profiles are typical of the distribution obtained at all speeds. Also shown in figure 10(a) are the average of the convex- and concave-surface design pressures at the tip position. In plotting the design pressures, it was assumed that the design inlet values were equal to those determined experimentally. The key in figure 10 gives the axial $(M_{2,z})$, the relative $(M_{2,R})$, and the absolute (M_2) exiting Mach numbers near the tip radius as calculated from the measurements taken behind the rotor. Increasing the back pressure results in an increase in the static pressure over the rotor casing. The static-pressure measurements do not specifically determine the

location and presence of shocks in the rotor. However, the profiles do indicate that there are compressions in the rotor even at open throttle.

The profiles in conjunction with the calculated exit Mach numbers also indicate two types of operation. In one type of operation, the absolute axial-flow component $M_{2,z}$ leaving the rotor is supersonic as well as the absolute Mach number M_2 (for example, the flow at 81 percent and 101 percent of design speed at minimum back pressure). In another type of operation, the absolute axial-flow component $M_{2,z}$ leaving the rotor is subsonic while the absolute Mach number M_2 is supersonic (for example, the flow with increased back pressure at 81 percent of design speed). For the subsonic axial case $M_{2,z} < 1$, a strong shock must be located either in the rotor passage or in the annulus at the rear of the rotor. When the absolute axial Mach number $M_{2,z}$ is supersonic, the efficiency would be expected to decrease when the back pressure is increased since the shock loss at the rear of the rotor is increasing. However, when the axial exit Mach number $M_{2,z}$ is subsonic, the shock may be located in the rotor and an increase in back pressure may increase the efficiency as the Mach number before the shock in the rotor may decrease and thus decrease the shock loss. As a result of this behavior, the overall efficiency has the characteristic that efficiency decreases with an increase in back pressure for the two highest speeds and for the lowest three speeds the efficiency decreased with increasing back pressure and then increased with a further increase in back pressure.

Blade-Element Performance

The radial distribution of several rotor-performance parameters is presented in figures 11 to 17 for 62 percent, 81 percent, 91 percent, and 101 percent of design speed. Only the minimum and maximum pressure conditions are presented.

Inlet conditions.- The relative inlet flow angles shown in figure 11 are greater than the design values; for example, they are 5° greater at the pitch. Therefore, the rotor operated at a positive angle, herein defined as the angle between the relative upstream undisturbed flow direction and the straight portion of the suction surface near the leading edge. As can be seen from figure 12, the tip relative inlet Mach number for these tests varied from approximately 0.94 to 1.53 with only slight changes due to throttling. At the design speed, the inlet Mach numbers were lower than the design values; for example, approximately 0.1 and 0.2 lower, respectively, at the pitch and tip sections. The measured axial inlet Mach number was 0.66 instead of the design value of 0.8; and the equivalent weight flow was approximately 28.6 instead of the design value

of 31.1 lb/sec of air per square foot of frontal area. The reason for the differences between the measured and the design condition cannot be determined exactly; however, these differences can be attributed partly to the fact that the rotor leading edge is blunt instead of sharp as was assumed in the design. The effect of the leading edge of the blade is extended upstream through waves. This is in agreement with the two-dimensional analysis of reference 9 which shows that the Mach number entering a blade passage is different from the upstream Mach number when a finite wedge or radius is used to thicken the rotor leading edge.

Exit conditions.- Figure 13 shows the radial distribution of the absolute flow angle leaving the rotor. The average flow angle at 101 percent of the design speed and minimum back pressure is approximately equal to 45°. The radial variations of the relative Mach numbers and the absolute Mach numbers leaving the rotor are shown in figures 14 and 15, respectively. In general, the absolute Mach numbers and the relative Mach numbers show similar trends. For minimum back pressure, the Mach number is fairly uniform across the passage except for the fall-off near the hub and tip. The average absolute exit Mach number at design speed is approximately 2.4. For maximum back pressure, the region of fall-off increases; this indicates that there is an increase of the secondary flow region. This increase in the secondary flow region can be attributed to the effect of the shock or shocks that are located in the passage or in the annulus at the rear of the rotor when the maximum back pressure is applied. This idea is also supported by the forward movement of the pressure on the outside casing (fig. 10) with an increase in the back pressure.

The radial variation of the total-pressure ratio and the momentum efficiency is shown in figures 16 and 17, respectively. An examination of these figures shows that the greater losses occur near the tip and hub as indicated by the radial distribution of the exit Mach number. With maximum back pressure, the losses near the hub are greatly increased and indicate again that there is an increase in the secondary flow. For minimum back pressure, the momentum efficiencies indicate that there is nearly isentropic flow in the center of the passages and that the losses are mainly composed of hub and tip losses; whereas, for the maximum-back-pressure cases, the implications are that the shock losses in the center of the passage and the diffusion losses resulting from shock and boundary-layer interaction and the hub and tip losses are all significant.

Implication of design procedure from rotors tested.- Figure 18 shows calculations of the total-pressure ratio and efficiency for the two impulse rotors reported in references 8 and 9 and the rotor of this report. The data for all of these rotors were taken near design speed and minimum back pressure. Some additional parameters for these rotors at or near design speed are given in the following table:

Source of data	Design pressure ratio	Inlet hub-tip ratio	Experimental results	
			Pressure ratio	Efficiency, percent
Ref. 9	8.0 (isentropic)	0.710	6.25	80.4
Ref. 8	6.9 (isentropic)	.750	5.70	89
Present report	6.5 (rotor efficiency of 90 percent)	.575	7.20	90

No attempt will be made in this report to compare the relative merit of the three rotors. However, the following generalities are indicated by the data from these three rotors: (1) None of the existing methods of design can accurately predict the operation of a supersonic impulse rotor. It appears that the design procedure used for the rotor reported in this paper is as satisfactory as the other methods. (2) Although the present methods of design do not accurately determine the operating conditions, rotors designed by any of these methods impart a large work output to the air in the form of kinetic energy. (3) Although the rotors indicate good performance, the performance of the complete compressor will depend to a large extent on the efficient recovery of the kinetic energy in the stators. The exit conditions for these rotors appear to be sufficiently uniform in angle, Mach number, and total pressure to allow possible efficient recovery in the stators. However, there are not sufficient stator data to predict accurately the final results.

SUMMARY OF RESULTS

A 16-inch-diameter supersonic impulse rotor with guide vanes was designed and tested in Freon-12. The rotor had inlet and exit hub-tip radius ratios of 0.575 and 0.75, respectively. The blade-passage design was based on a two-dimensional vortex-flow theory modified to account partially for the three-dimensional compressions. The following results were obtained in the investigation of this rotor:

1. Near the design tip speed of 662 ft/sec in Freon-12 (equivalent air value of 1,450 ft/sec) and minimum back pressure, the rotor produced a stagnation-pressure ratio of 7.2 and an efficiency of 90 percent with an equivalent weight flow of 28.6 lb/sec of air per square foot of frontal area.

2. The efficiency at minimum back pressure was approximately constant at 90 percent for all speeds.

3. The stagnation-pressure ratio decreased with increasing back pressure. The maximum-back-pressure condition at design speed resulted in a pressure ratio of 5.4 and an efficiency of 77.5 percent. For high efficiency, a stator must therefore operate without imposing a high back pressure on the rotor.

4. The average exit Mach number at design speed and minimum back pressure was approximately 2.4 at an average discharge angle of 45°.

5. The operating conditions were not accurately predicted by the design method, but the resulting rotor imparts a large work output to the fluid in the form of kinetic energy. The exit conditions for this rotor appear to be sufficiently uniform in flow angle, Mach number, and total pressure to allow possible efficient recovery in the stators.

Langley Aeronautical Laboratory,
National Advisory Committee for Aeronautics,
Langley Field, Va., December 31, 1957.

REFERENCES

1. Kantrowitz, Arthur: The Supersonic Axial-Flow Compressor. NACA Rep. 974, 1950. (Supersedes NACA ACR L6D02.)

2. Ferri, Antonio: Preliminary Analysis of Axial-Flow Compressors Having Supersonic Velocity at the Entrance of the Stator. NACA RM L9G06, 1949.

3. Wright, Linwood C., and Klapproth, John F.: Performance of Supersonic Axial-Flow Compressors Based on One-Dimensional Analysis. NACA RM E8L10, 1949.

4. Liccini, Luke L.: Analytical and Experimental Investigation of 90° Supersonic Turning Passages Suitable for Supersonic Compressors or Turbines. NACA RM L9G07, 1949.

5. Boxer, Emanuel, Sterrett, James R., and Wlodarski, John: Application of Supersonic Vortex-Flow Theory to the Design of Supersonic Impulse Compressor- or Turbine-Blade Sections. NACA RM L52B06, 1952.

6. Goldstein, Arthur W.: Axisymmetric Supersonic Flow in Rotating Impellers. NACA Rep. 1083, 1952. (Supersedes NACA TN 2388.)

7. Ullman, Guy N., Hartmann, Melvin J., and Tysl, Edward R.: Experimental Investigation of a 16-Inch Impulse-Type Supersonic-Compressor Rotor. NACA RM E51G19, 1951.

8. Tysl, Edward R., Klapproth, John F., and Hartmann, Melvin J.: Investigation of a Supersonic-Compressor Rotor With Turning to Axial Direction. I - Rotor Design and Performance. NACA RM E53F23, 1953.

9. Goldstein, Arthur W., and Schacht, Ralph L.: Performance of a Swept Leading Edge Rotor of the Supersonic Type With Mixed Flow. NACA RM E52K03, 1953.

10. Costilow, Eleanor L.: Application of a Characteristic Blade-to-Blade Solution to Flow in a Supersonic Rotor With Varying Stream-Filament Thickness. NACA TN 2992, 1953.

11. Goldberg, Theodore J., Boxer, Emanuel, and Bernot, Peter T.: Experimental Investigation of an Axial-Flow Supersonic Compressor Having Rounded Leading-Edge Blades With an 8-Percent Mean Thickness-Chord Ratio. NACA RM L53G16, 1953.

TABLE I

COORDINATES OF COMPRESSOR BLADES

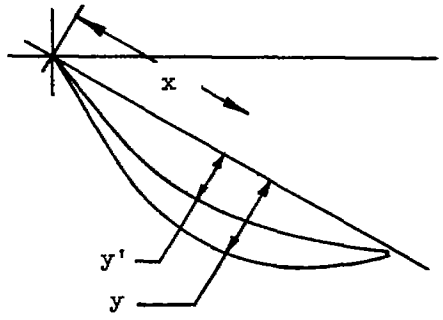

Section A-A (See fig. 5.)			Section B-B (See fig. 5.)			Section C-C (See fig. 5.)		
x, in.	y, in.	y', in.	x, in.	y, in.	y', in.	x, in.	y, in.	y', in.
0	0	0	0	0	0	0.045	0.077	0.051
.126	.086	.055	.076	.090	.056	.142	.205	.156
.221	.144	.102	.283	.276	.218	.285	.359	.285
.443	.261	.201	.567	.516	.408	.427	.541	.415
.664	.381	.290	.709	.638	.487	.570	.687	.521
.886	.498	.378	.851	.760	.556	.712	.841	.607
1.107	.613	.471	.993	.874	.617	.855	.946	.672
1.329	.720	.542	1.135	.976	.663	.998	1.053	.729
1.550	.832	.589	1.277	1.050	.695	1.140	1.140	.778
1.772	.925	.613	1.419	1.112	.709	1.283	1.214	.812
1.993	1.014	.635	1.561	1.163	.720	1.425	1.271	.835
2.215	1.069	.640	1.703	1.193	.721	1.607	1.324	.848
2.436	1.107	.637	1.845	1.215	.726	1.710	1.346	.852
2.658	1.120	.617	1.987	1.229	.721	1.853	1.354	.855
2.879	1.114	.591	2.185	1.22	.699	1.996	1.351	.846
3.101	1.089	.562	2.271	1.215	.689	2.138	1.337	.826
3.322	1.041	.522	2.442	1.170	.664	2.281	1.297	.795
3.544	.968	.478	2.554	1.135	.644	2.442	1.234	.748
3.765	.875	.432	2.700	1.064	.605	2.566	1.180	.715
3.987	.753	.372	2.838	.986	.570	2.709	1.106	.661
4.209	.593	.296	3.122	.797	.496	2.851	1.012	.613
4.430	.416	.205	3.264	.715	.454	2.994	.901	.553
4.500	.357	.177	3.406	.618	.405	3.136	.797	.499
4.628	.249	.115	3.548	.533	.359	3.422	.593	.376
4.692	.192	.086	3.690	.445	.295	3.707	.382	.239
4.782	.087	.087	3.832	.354	.229	3.992	.182	.079
			3.974	.269	.163	4.134	.071	0
			4.191	.128	.051	4.180	.028	.028
			4.281	.079	0			
			4.339	.024	.024			

TABLE II

COORDINATES OF COMPRESSOR HUB

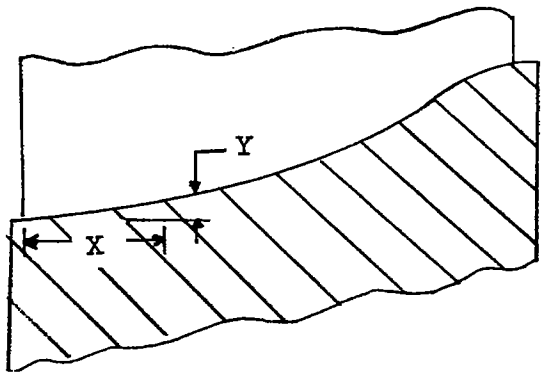

X, in.	Y, in.
0	0
.500	.050
1.000	.110
1.500	.183
2.000	.290
2.500	.513
3.000	.793
3.500	1.100
4.000	1.360
4.150	1.400

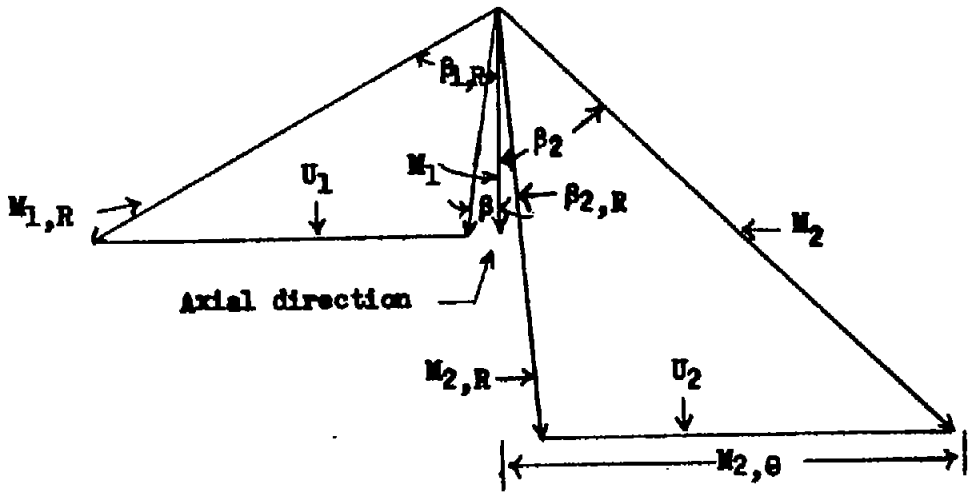

r_1, ft	r_2, ft	M_1	β_1, deg	$M_{1,R}$	$\beta_{1,R}$, deg	$M_{2,R}$	$\beta_{2,R}$, deg	M_2	β_2, deg	p_2/p_1	P_2/P_i
.667	.667	.795	- 9.5	1.70	-62.6	1.46	2.4	2.03	44.1	1.16	6.5
.525	.592	.800	-12.0	1.48	-58.0	1.54	14.9	2.19	47.3	.86	6.5
.383	.517	.810	-16.2	1.29	-52.5	1.72	27.9	2.43	51.3	.56	6.5

Figure 1.- Velocity diagram for design conditions in Freon-12.

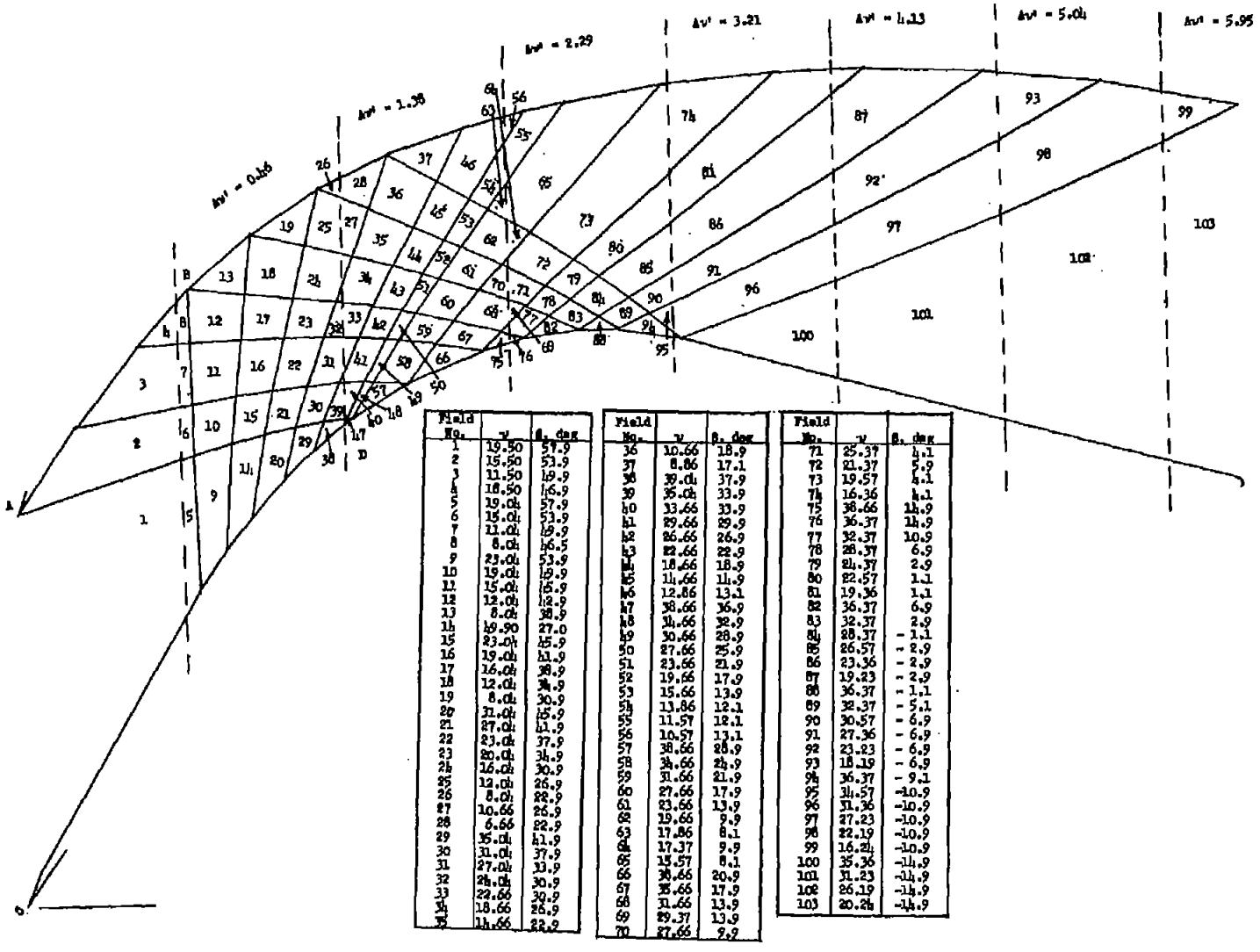

Field No.	ν	θ, deg
1	19.50	57.9
2	15.50	53.9
3	11.50	49.9
4	18.50	46.9
5	19.04	57.9
6	15.04	53.9
7	11.04	49.9
8	8.04	46.5
9	23.04	53.9
10	19.04	49.9
11	15.04	45.9
12	12.04	42.9
13	8.04	38.9
14	49.90	27.0
15	23.04	45.9
16	19.04	41.9
17	16.04	38.9
18	12.04	34.9
19	8.04	30.9
20	31.04	45.9
21	27.04	41.9
22	23.04	37.9
23	20.04	34.9
24	16.04	30.9
25	12.04	26.9
26	8.04	22.9
27	10.66	26.9
28	6.66	22.9
29	35.04	41.9
30	31.04	37.9
31	27.04	33.9
32	24.04	30.9
33	22.66	30.9
34	18.66	26.9
35	14.66	22.9

Field No.	ν	θ, deg
36	10.66	18.9
37	8.86	17.1
38	39.04	37.9
39	35.04	33.9
40	33.66	33.9
41	29.66	29.9
42	26.66	26.9
43	22.66	22.9
44	18.66	18.9
45	14.66	14.9
46	12.86	13.1
47	38.66	36.9
48	34.66	32.9
49	30.66	28.9
50	27.66	25.9
51	23.66	21.9
52	19.66	17.9
53	15.66	13.9
54	13.86	12.1
55	11.57	12.1
56	10.57	13.1
57	38.66	28.9
58	34.66	24.9
59	31.66	21.9
60	27.66	17.9
61	23.66	13.9
62	19.66	9.9
63	17.86	8.1
64	17.37	9.9
65	13.57	8.1
66	38.66	20.9
67	35.66	17.9
68	31.66	13.9
69	29.37	13.9
70	27.66	9.9

Field No.	ν	θ, deg
71	25.37	4.1
72	21.37	5.9
73	19.57	4.1
74	16.36	4.1
75	38.66	14.9
76	36.37	14.9
77	32.37	10.9
78	28.37	6.9
79	24.37	2.9
80	22.57	1.1
81	19.36	1.1
82	36.37	6.9
83	32.37	2.9
84	28.37	- 1.1
85	26.57	- 2.9
86	23.36	- 2.9
87	19.23	- 2.9
88	36.37	- 1.1
89	32.37	- 5.1
90	30.57	- 6.9
91	27.36	- 6.9
92	23.23	- 6.9
93	18.19	- 6.9
94	36.37	- 9.1
95	34.57	-10.9
96	31.36	-10.9
97	27.23	-10.9
98	22.19	-10.9
99	16.24	-10.9
100	35.36	-14.9
101	31.23	-14.9
102	26.19	-14.9
103	20.24	-14.9

Figure 2.- Illustration of modified two-dimensional characteristic network.

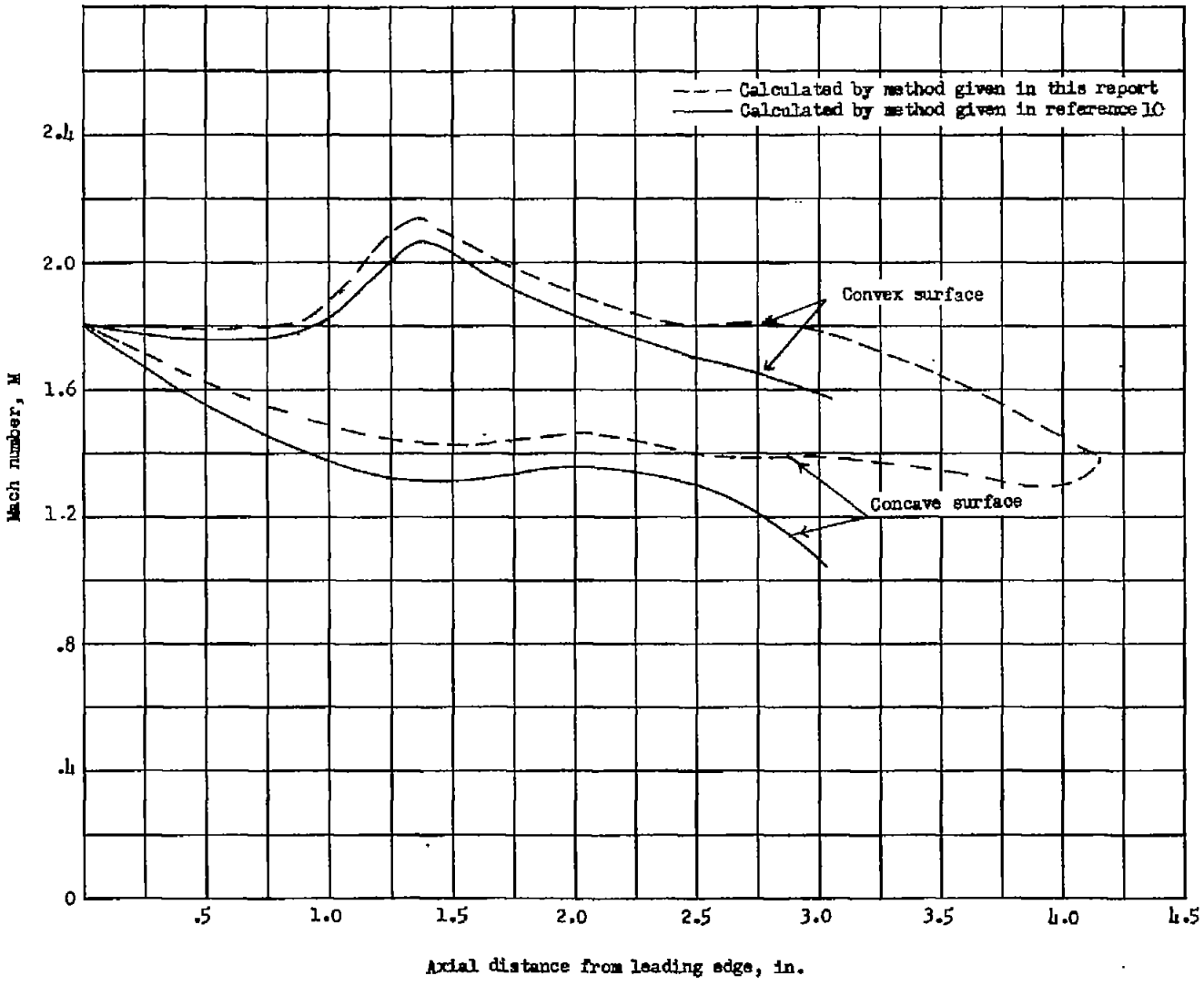

Figure 3.- Calculated Mach number distribution at tip section of blade.

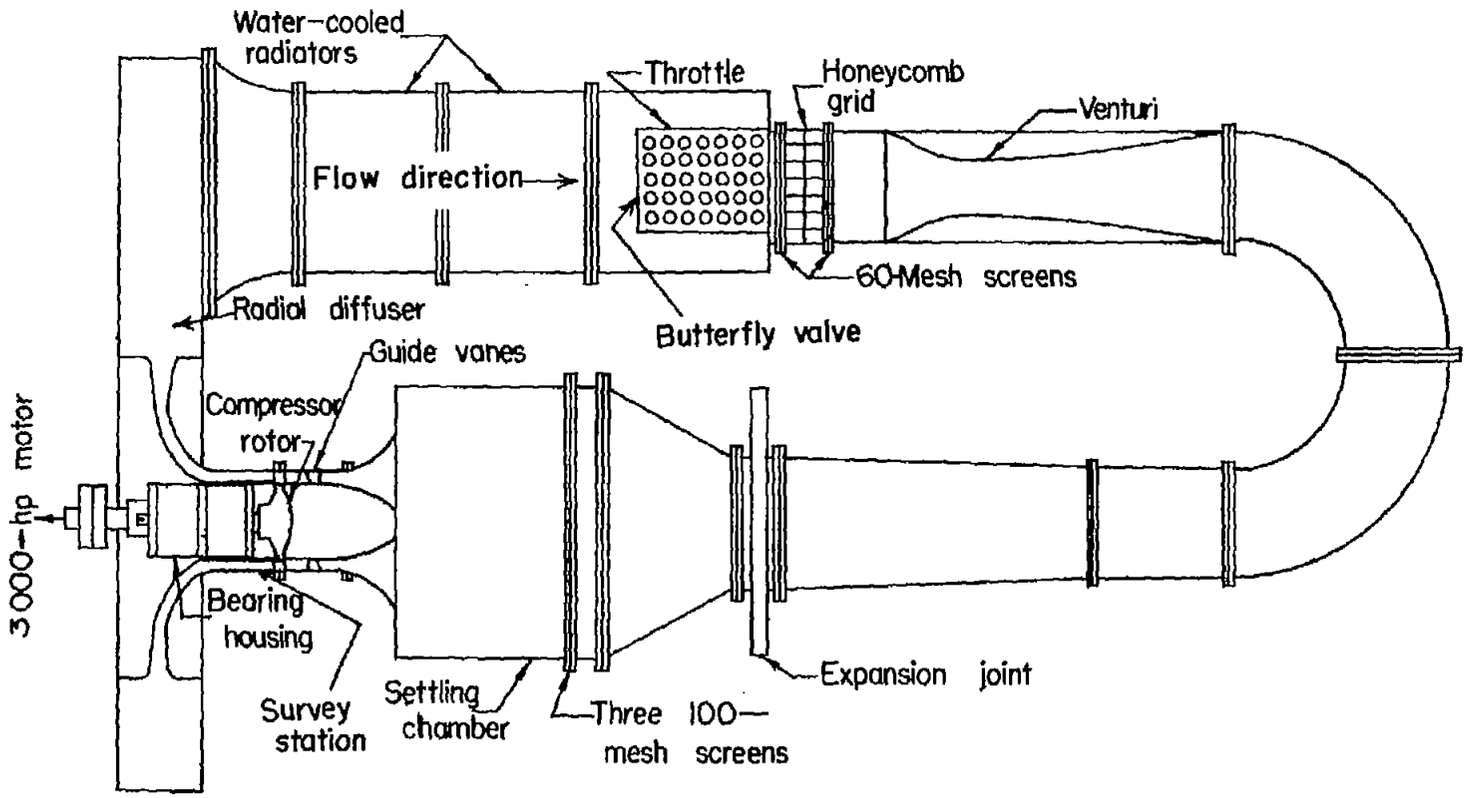

Figure 4.- Schematic drawing of supersonic-compressor test rig.

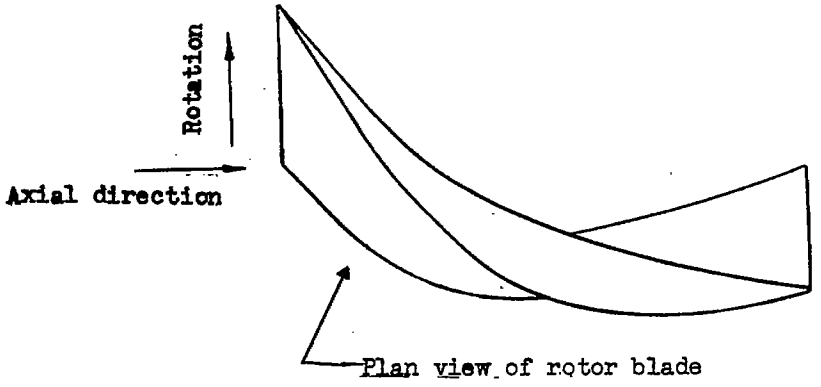

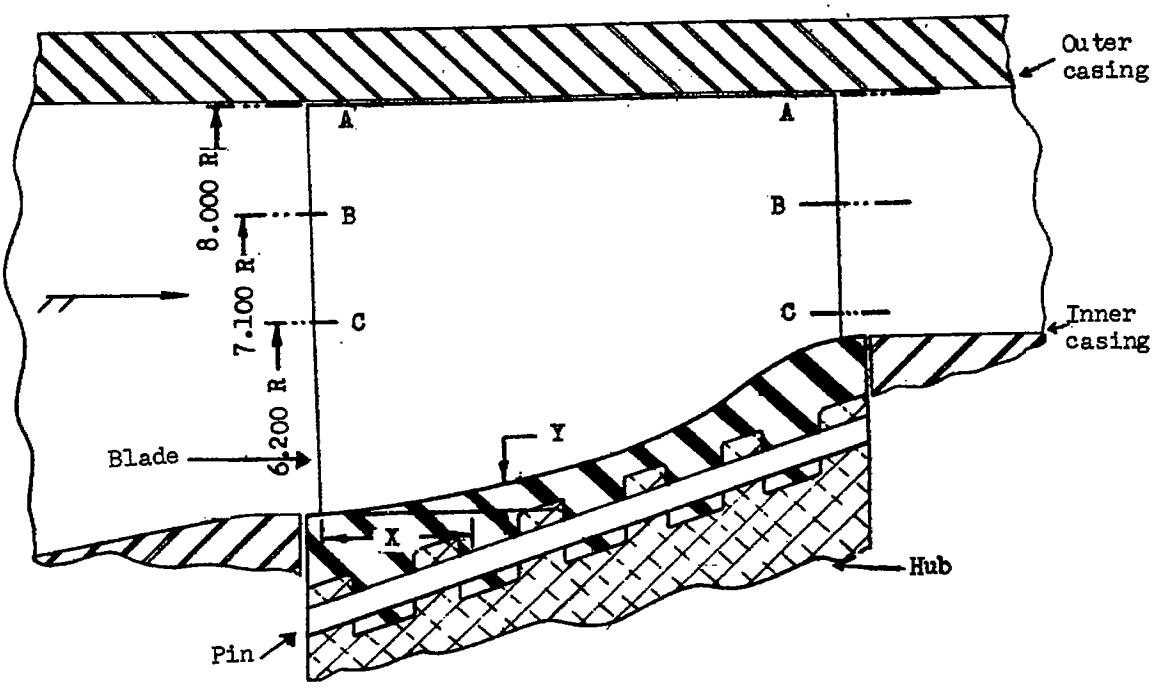

Figure 5.- Schematic drawing of rotor blade.

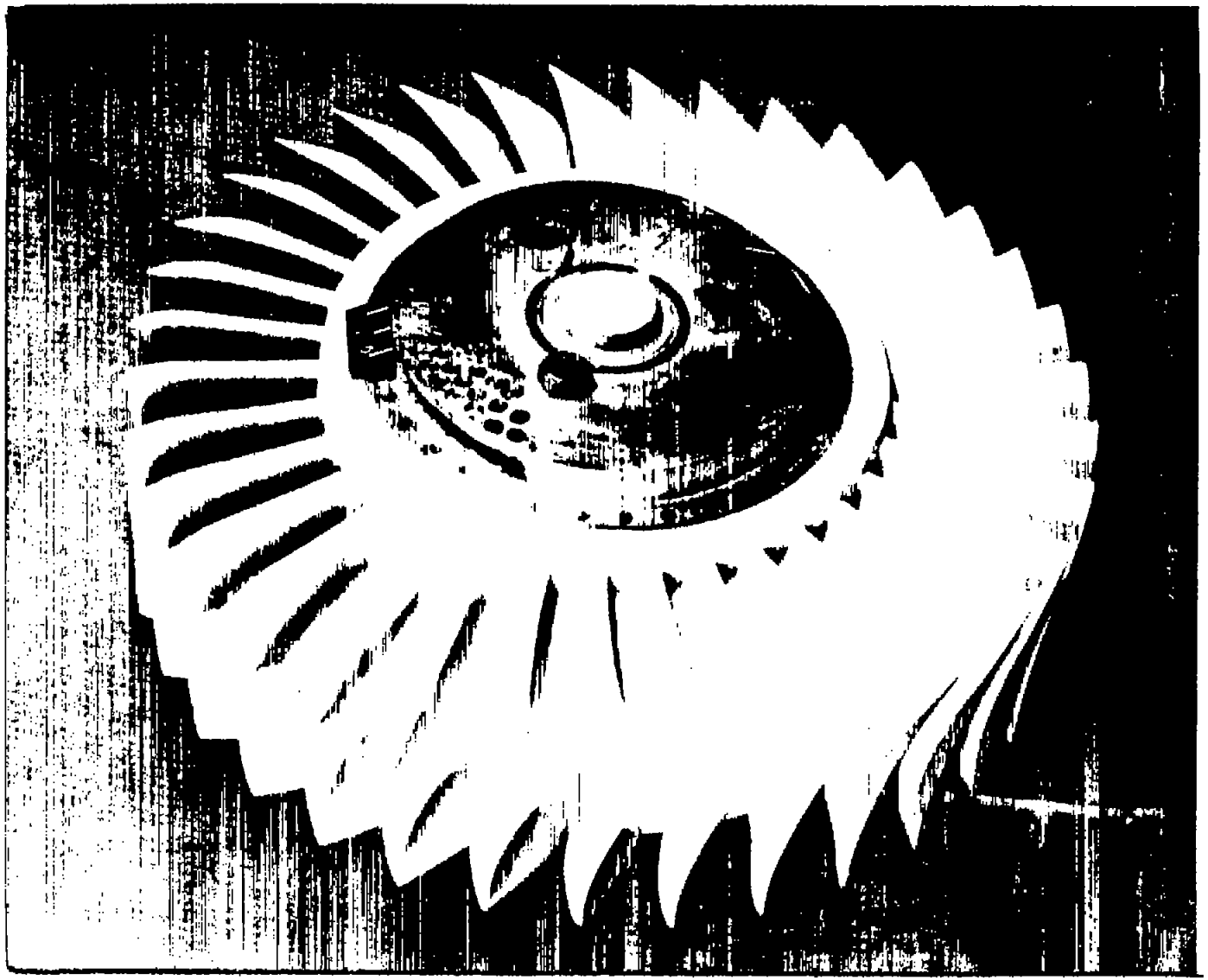

Figure 6.- Photograph of rotor. L-92658

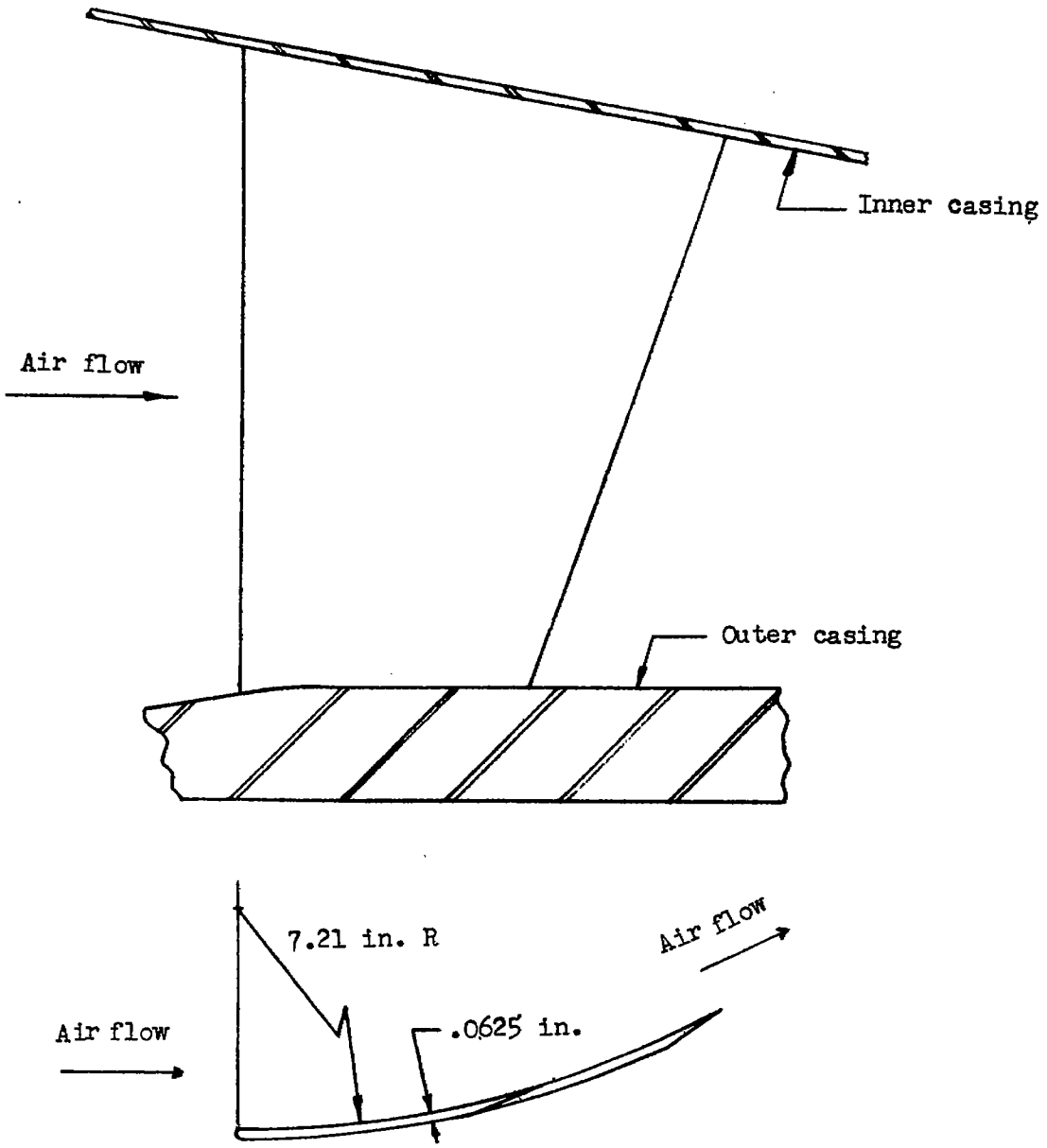

Figure 7.- Schematic drawing of guide vane.

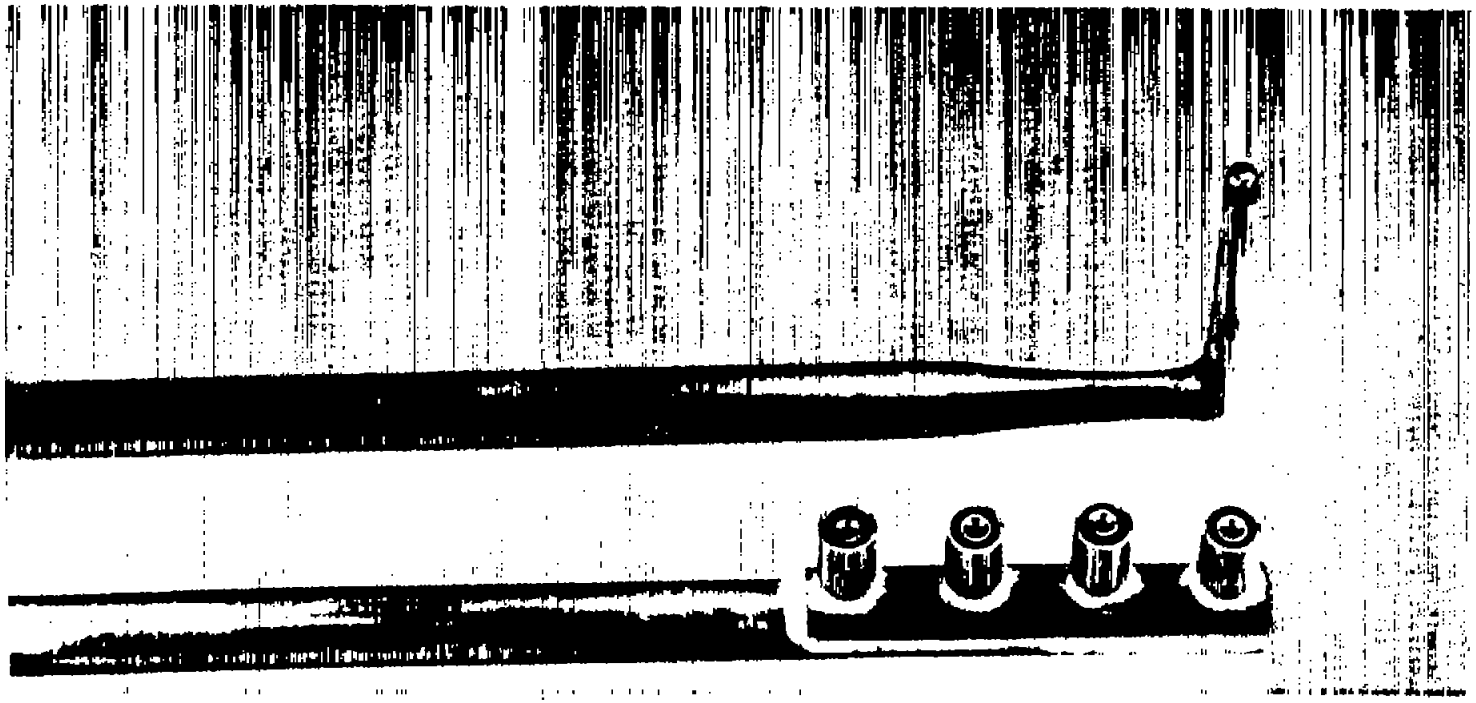

Figure 8.- Total-pressure and total-temperature probes. L-77481

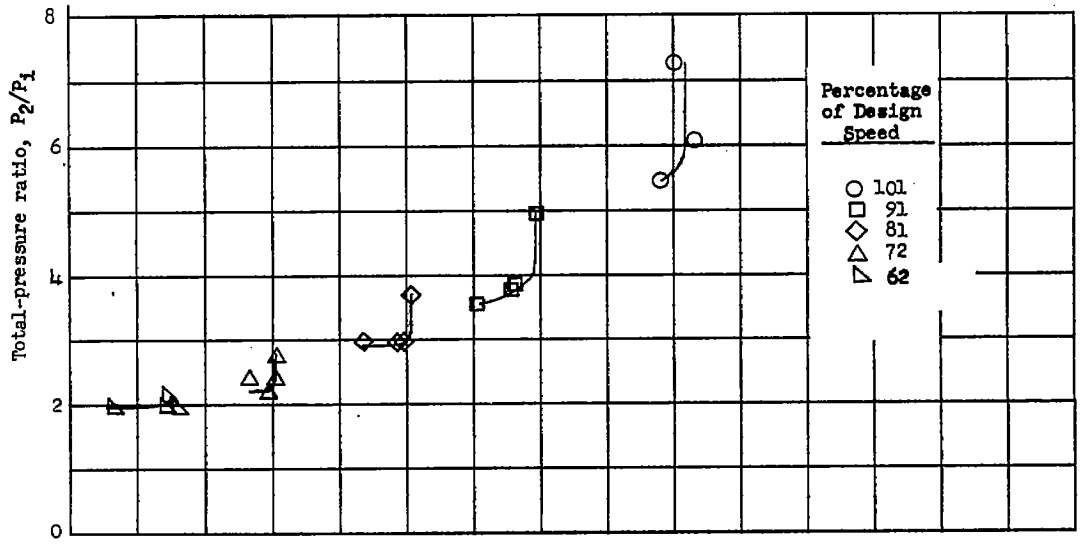

(a) Total-pressure ratio plotted against weight flow.

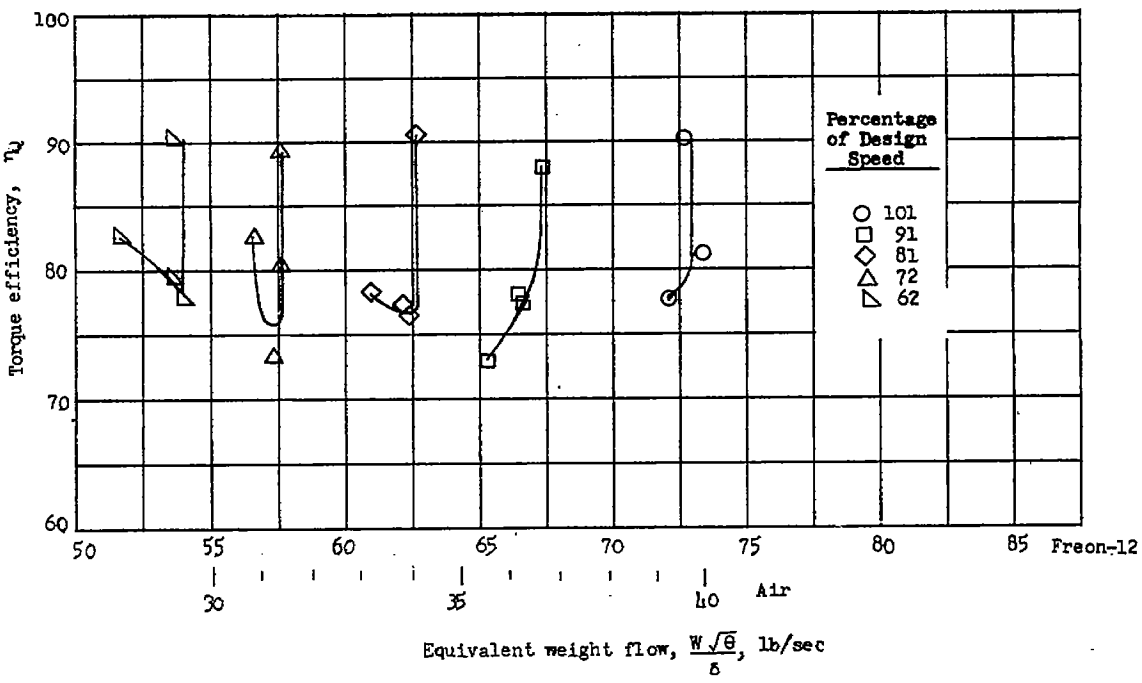

(b) Torque efficiency plotted against weight flow.

Figure 9.- Performance characteristics of rotor.

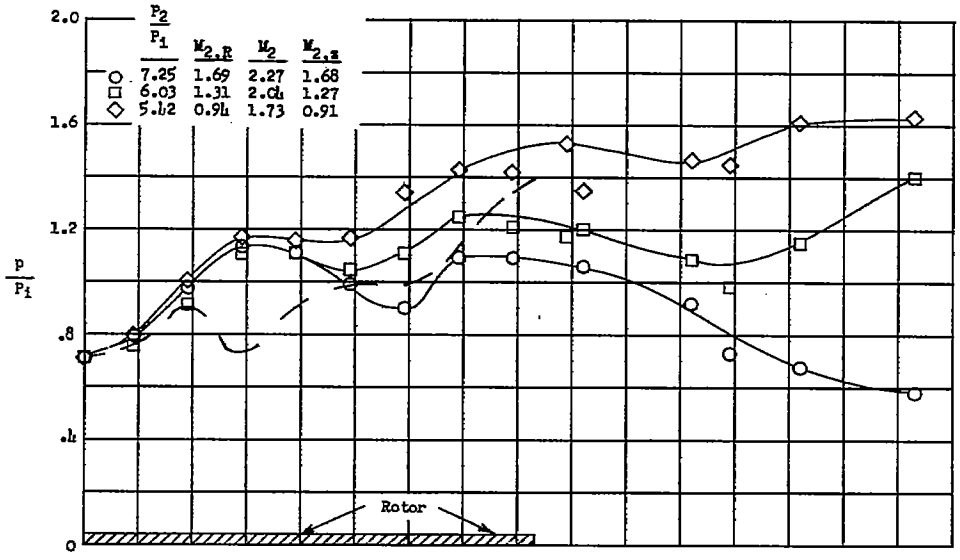

(a) 101 percent of design speed.

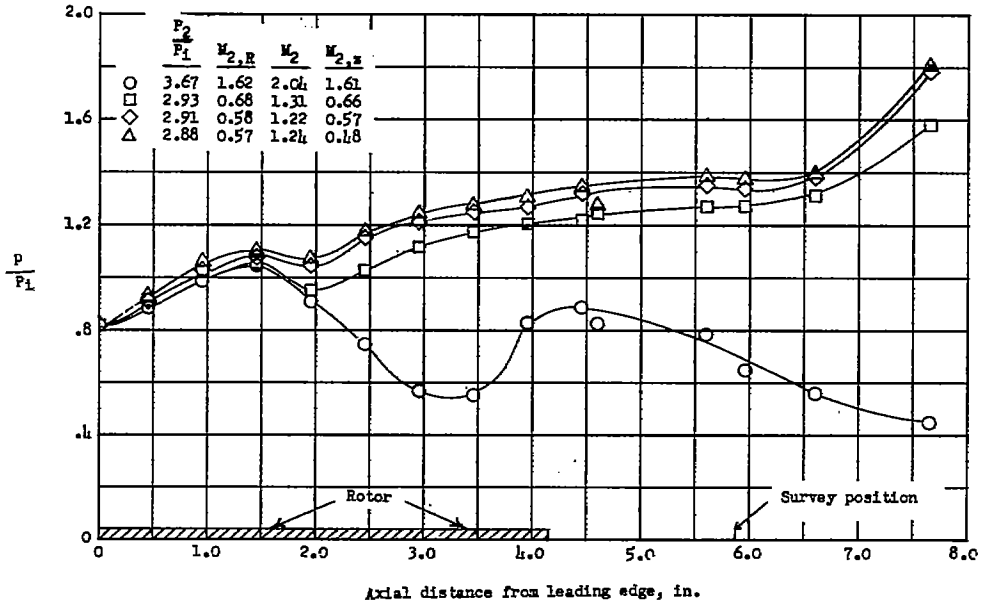

(b) 81 percent of design speed.

Figure 10.- Effect of back pressure on static-pressure distribution along outer casing. (Dashed line is design pressure at tip position.)

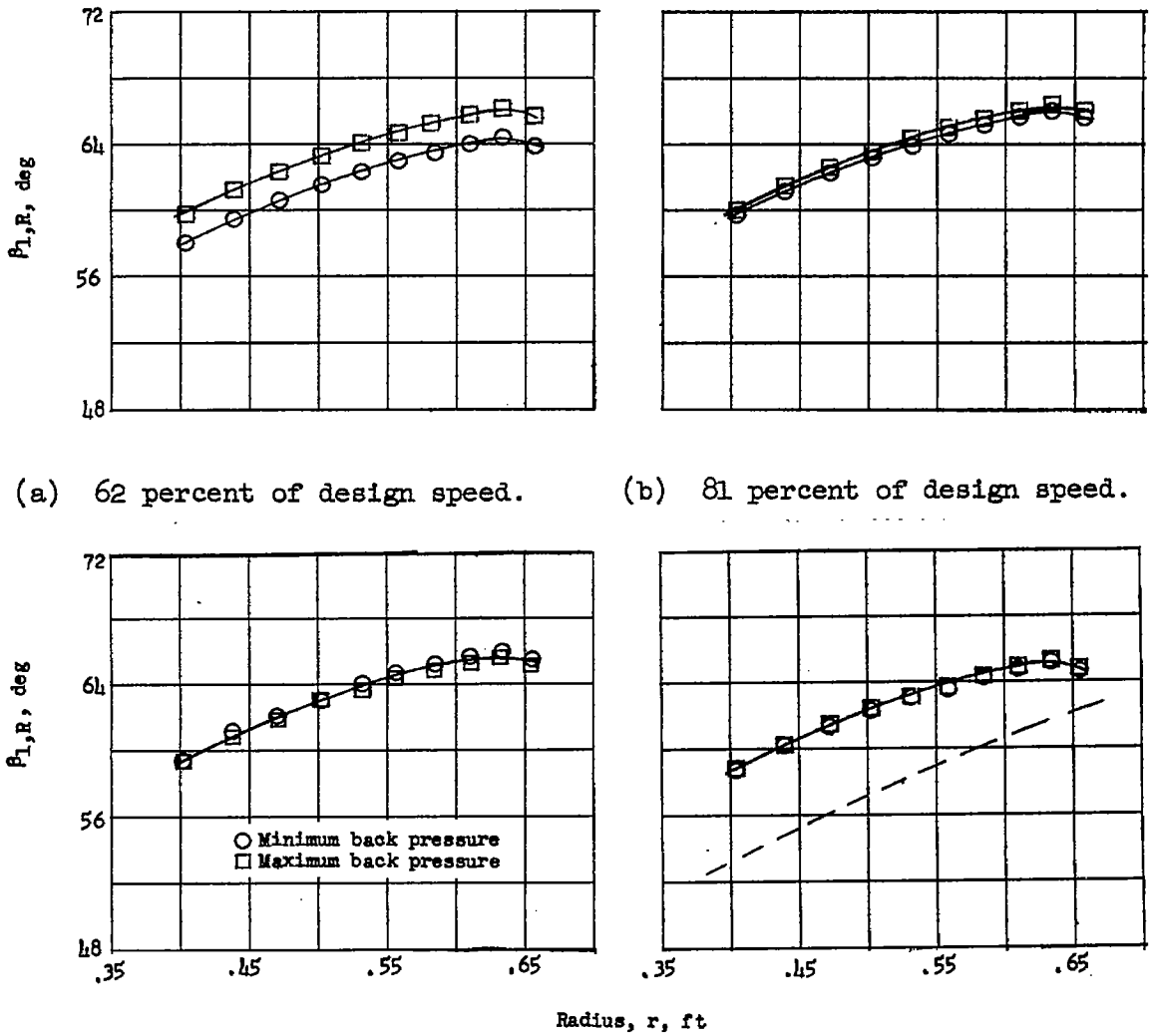

(a) 62 percent of design speed.

(b) 81 percent of design speed.

(c) 91 percent of design speed.

(d) 101 percent of design speed.

Figure 11.- Radial variation of relative inlet flow angle. (Design values are given by dashed line.)

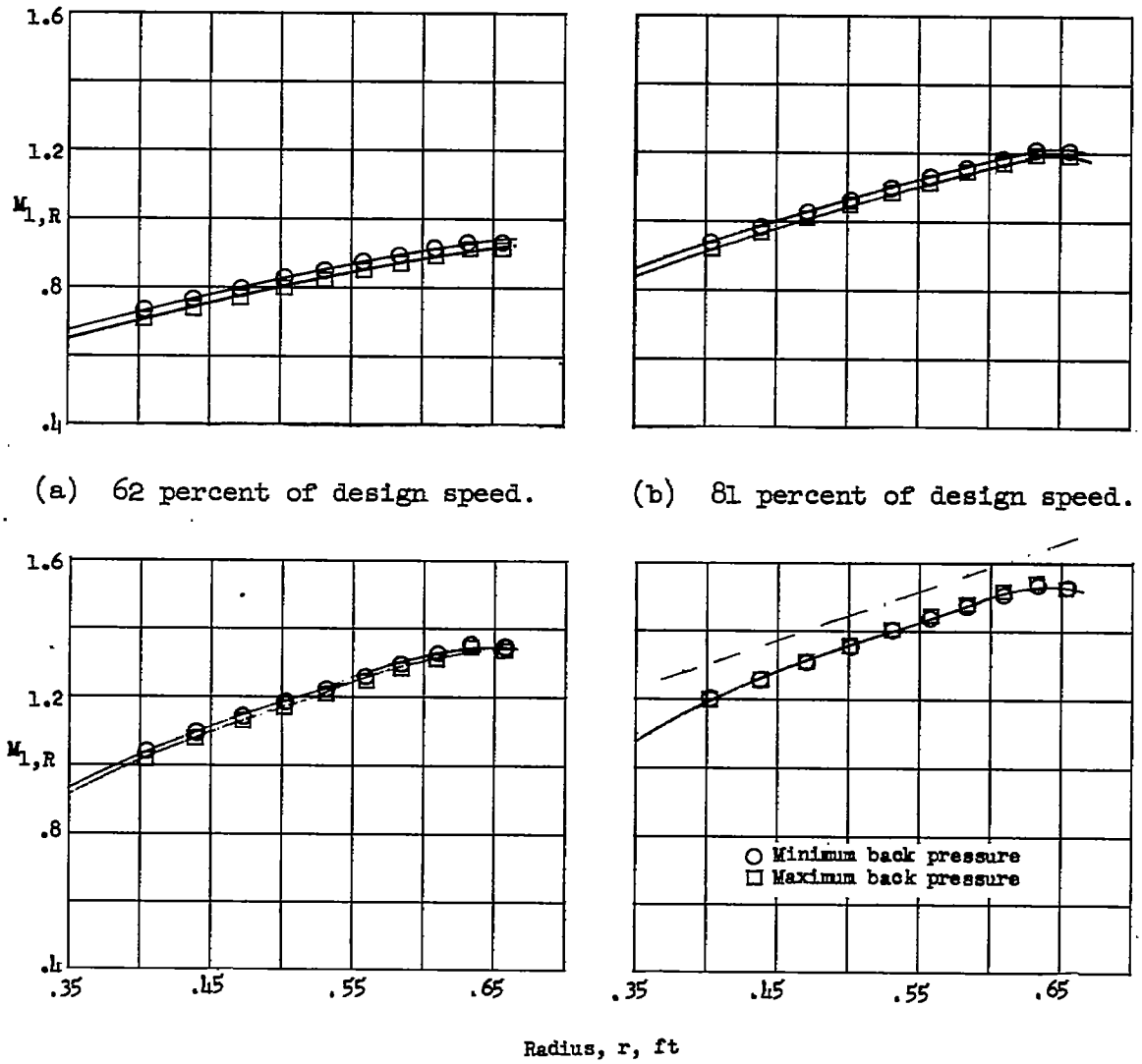

(a) 62 percent of design speed.

(b) 81 percent of design speed.

(c) 91 percent of design speed.

(d) 101 percent of design speed.

Figure 12.- Radial variations of inlet flow. (Design values are given by dashed line.)

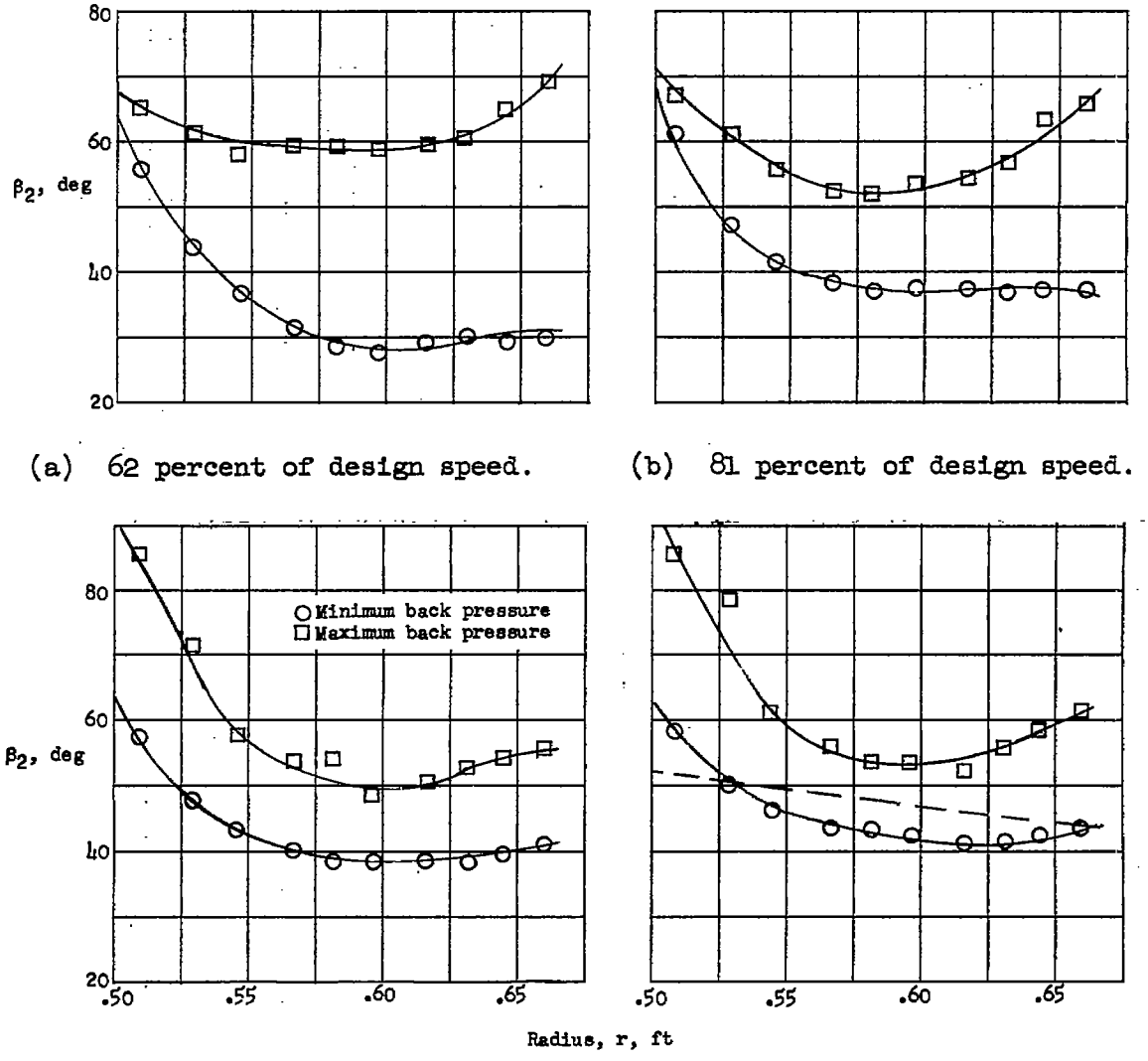

(a) 62 percent of design speed.

(b) 81 percent of design speed.

(c) 91 percent of design speed.

(d) 101 percent of design speed.

Figure 13.- Radial variation of absolute flow angle leaving rotor. (Design values are given by dashed line.)

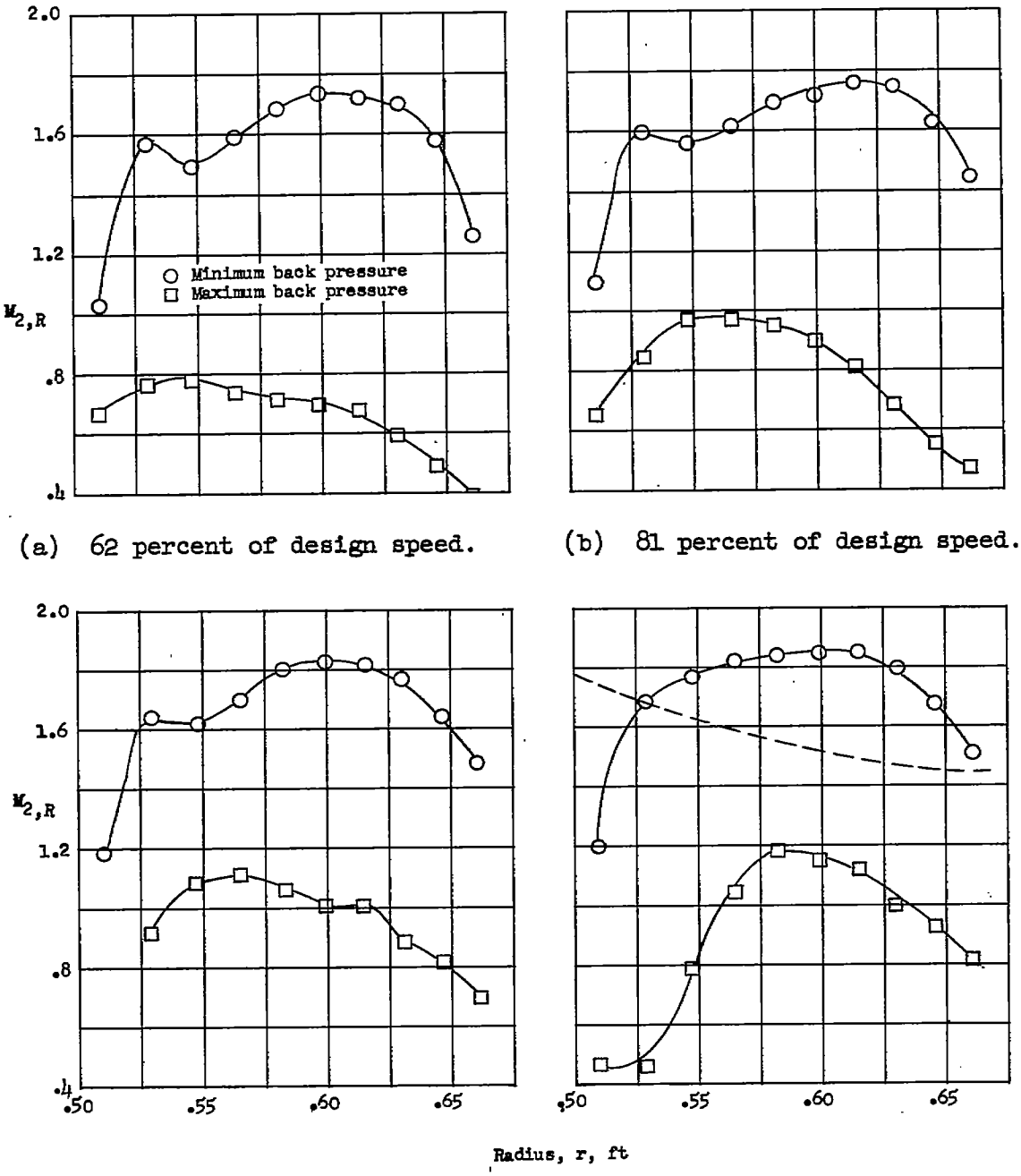

(a) 62 percent of design speed.

(b) 81 percent of design speed.

(c) 91 percent of design speed.

(d) 101 percent of design speed.

Figure 14.- Radial variation of relative exit flow. (Design values are given by dashed line.)

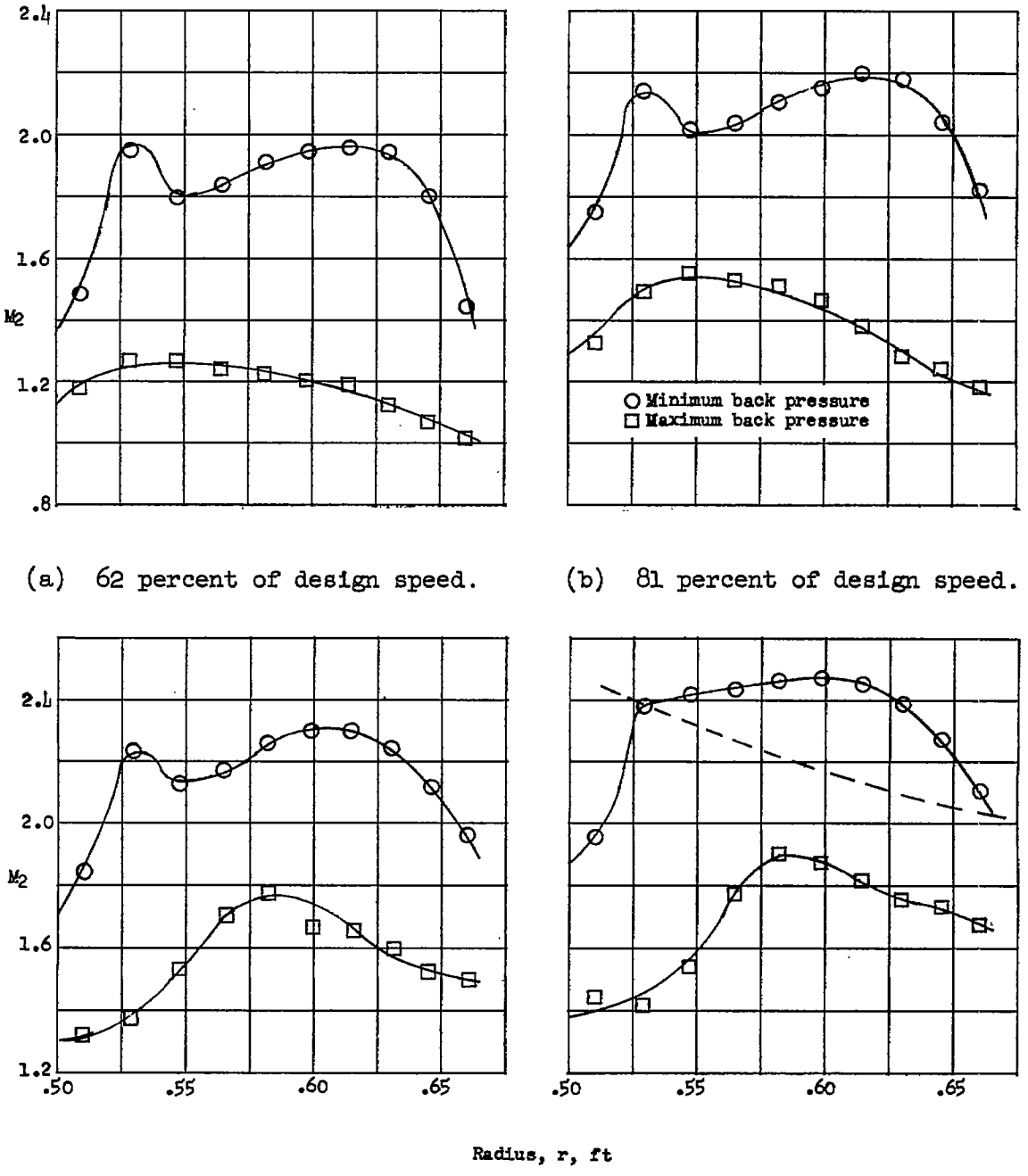

(a) 62 percent of design speed.

(b) 81 percent of design speed.

(c) 91 percent of design speed.

(d) 101 percent of design speed.

Figure 15.- Radial variation of absolute Mach number leaving rotor. (Design values are given by dashed line.)

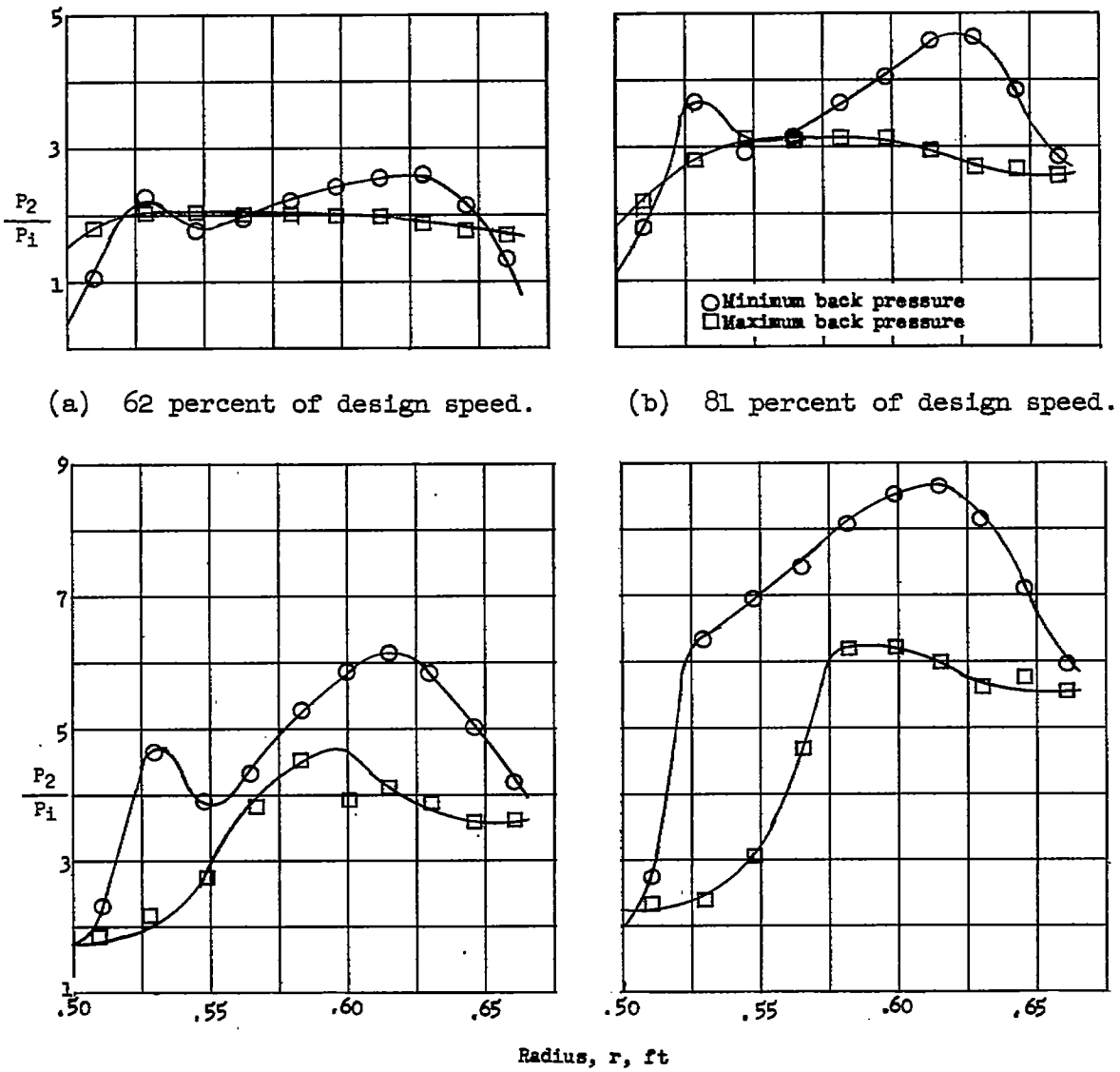

(a) 62 percent of design speed.

(b) 81 percent of design speed.

(c) 91 percent of design speed.

(d) 101 percent of design speed.

Figure 16.- Radial variation of total-pressure ratio.

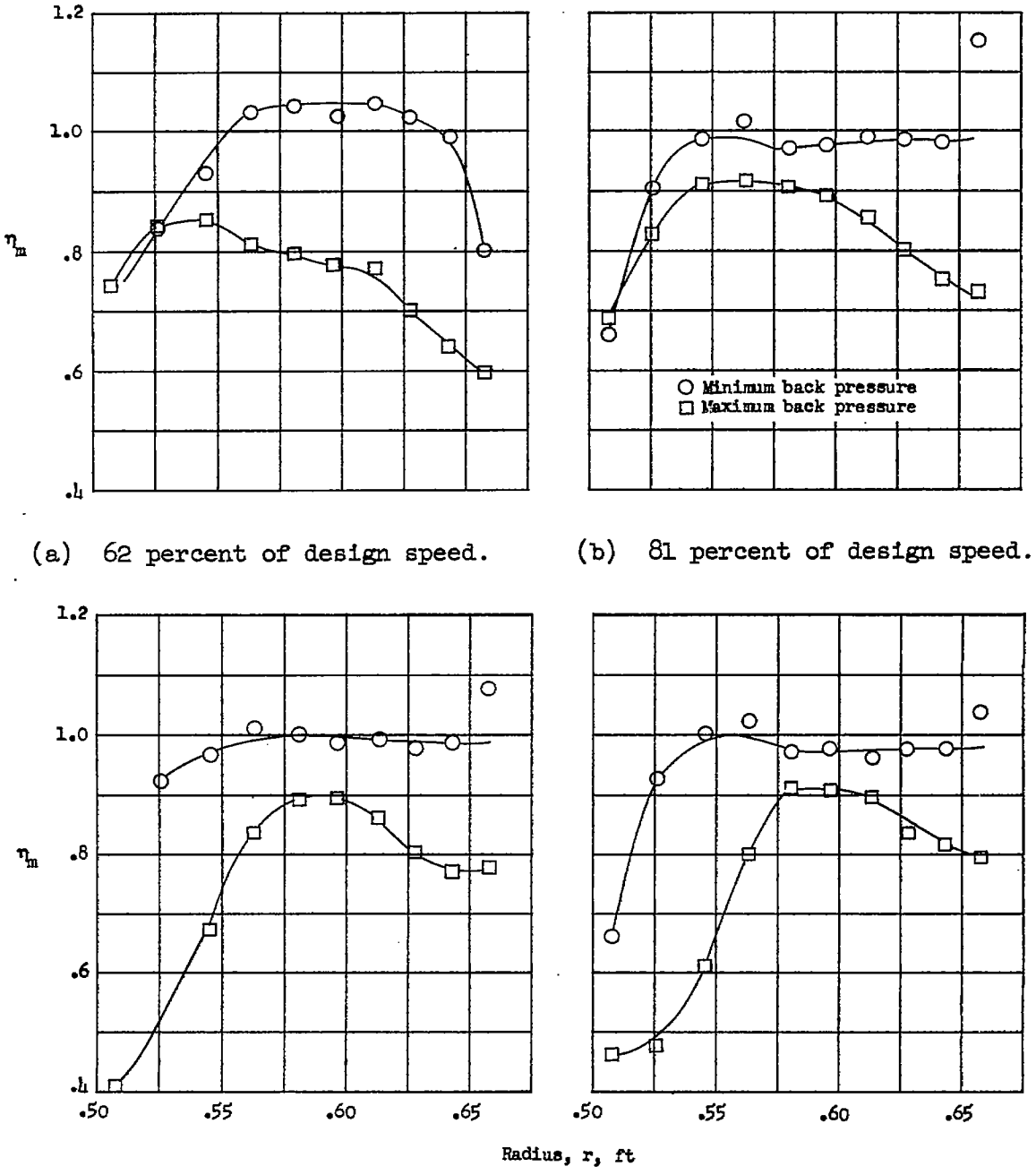

(a) 62 percent of design speed.

(b) 81 percent of design speed.

(c) 91 percent of design speed.

(d) 101 percent of design speed.

Figure 17.- Radial variation of efficiency based on momentum change.

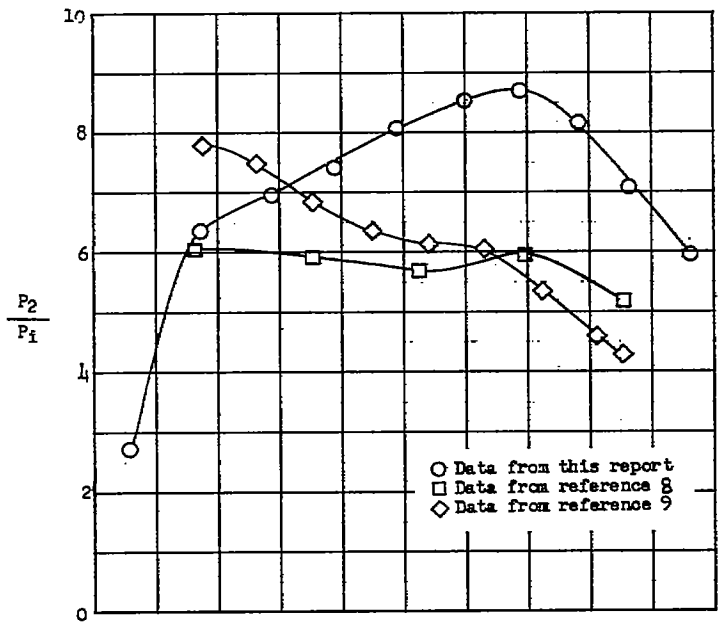

(a) Pressure ratio.

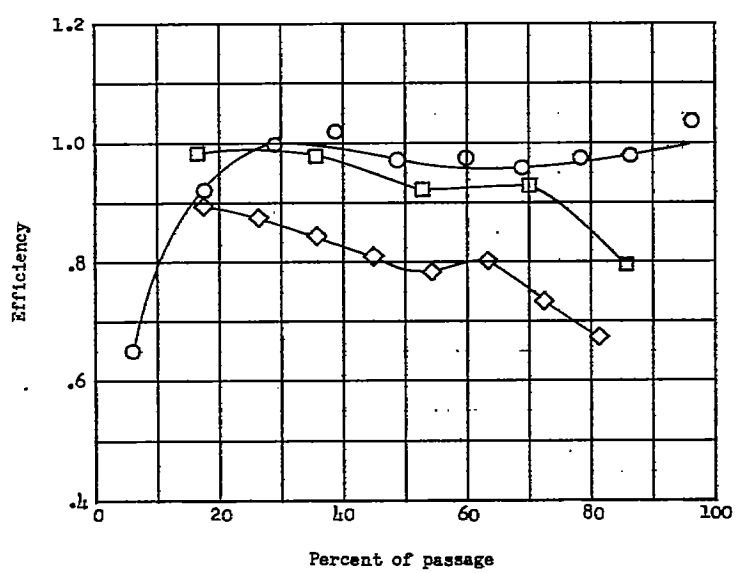

(b) Efficiency.

Figure 18.- Discharge conditions near design speed at open throttle for three impulse rotors.